

# NUMERICAL SIMULATIONS OF THE LAGRANGIAN AVERAGED NAVIER-STOKES (LANS- $\alpha$ ) EQUATIONS FOR FORCED HOMOGENEOUS ISOTROPIC TURBULENCE

Kamran Mohseni

Mail-code 107-81, Division of Engineering and Applied Science  
California Institute of Technology  
Pasadena, CA 91125

Steve Shkoller and Branko Kosović

Department of Mathematics,  
University of California, Davis, CA 95616-8633

Jerrold E. Marsden

Mail-code 107-81, Division of Engineering and Applied Science  
California Institute of Technology  
Pasadena, CA 91125

## ABSTRACT

The modeling capabilities of the Lagrangian Averaged Navier-Stokes- $\alpha$  equations (LANS- $\alpha$ ) is investigated in statistically stationary three-dimensional homogeneous and isotropic turbulence. The predictive abilities of the LANS- $\alpha$  equations are analyzed by comparison with DNS data. Two different forcing techniques were implemented to model the energetics of the energy containing scales. The resolved flow is examined by comparison of the energy spectra of the LANS- $\alpha$  and the DNS computations; furthermore, the correlation between the vorticity and the eigenvectors of the rate of the resolved strain tensor is studied. We find that the LANS- $\alpha$  equations captures the gross features of the flow while the wave activity below a given scale  $\alpha$  is filtered by the non-linear dispersion.

## 1 INTRODUCTION

In the last three decades computers made highly accurate numerical simulations of the Navier-Stokes equations feasible for moderate Reynolds number flows. The capability of reproducing experimentally obtained data for various flows has been demonstrated by these simulations; see Rogallo and Moin<sup>1</sup> and Canuto *et al.*<sup>2</sup> for an earlier account on the progress in this area.

The behavior of small scales in turbulent flows is usually characterized by statistical isotropy, homogeneity, and universality. Consequently, by investigating the simplest turbulent flow, i.e. isotropic homogeneous turbulence, we hope to understand small scale turbulence. Isotropic homogeneous turbulence can be categorized as either decaying or forced. While the forced isotropic turbulence is usually designed to be statistically stationary, decaying turbulence is always statistically non-stationary.

Forced isotropic turbulence in a periodic box can be considered as one of the most basic numerically simulated turbulent flows. Forced isotropic turbulence is achieved by applying isotropic forcing to the low wave number modes so that the turbulent cascade develops as the statistical equilibrium is reached. Statistical equilibrium is signified by the balance between the input of kinetic energy through forcing and its output through the viscous dissipation. Isotropic forcing cannot be produced in a laboratory and therefore forced isotropic turbulence is an idealized flow configuration that can be achieved only via a controlled numerical experiment; nevertheless, forced isotropic turbulence represents an important test case for studying basic properties of turbulence in a statistical equilibrium.

It is generally believed that the Kolmogorov cascade theory<sup>3</sup> provides an approximate description of homogeneous isotropic turbulence. The almost universal scaling of the dissipation range in Kolmogorov variables and the  $k^{-5/3}$  energy spectrum are among

---

Copyright © 2001 by the authors. Published by the American Institute of Aeronautics and Astronautics, Inc. with permission.

the most successful predictions in turbulent flows.

Direct Numerical Simulation (DNS) of homogeneous isotropic turbulence is well established and has been extensively studied in the last three decades. Such computations can be used to probe features, examine statistics of quantities normally not available in conventional experiments, and test new turbulence models. The main difficulty in the turbulence engineering community is that performing the DNS of typical engineering problems (usually at high Reynolds numbers) is very expensive, and therefore unlikely to happen in the foreseeable future. There are methods for simulating turbulent flows where one does not need to use the brute-force approach of DNS to resolve all scales of motion. Two popular alternatives are the Large Eddy Simulation (LES) models and the Reynolds averaging of the Navier-Stokes equations, known as the (RANS) equations.

In this paper, we shall numerically investigate the LANS- $\alpha$  equations in the subgrid-stress form introduced by Marsden and Shkoller (2001); the inviscid form of these equations on all of  $\mathbb{R}^3$  were introduced in Holm *et al.*(1998) and on compact manifolds in Shkoller (1998). Unlike the traditional averaging or filtering approach used for both the RANS and the LES, wherein the Navier-Stokes equations are averaged, the LANS- $\alpha$  approach is based on averaging at the level of the variational principle from which the Euler equations are derived. Namely, a new averaged action principle is defined. The least action principle then yields the so-called Lagrangian-Averaged Euler (LAE- $\alpha$ ) equations. The Lagrangian-Averaged Navier-Stokes equations (LANS- $\alpha$ ) are obtained by allowing the Lagrangian flow to be stochastic and replacing deterministic time derivatives with stochastic back-in-time mean derivatives; the viscous diffusion term naturally arises in this fashion. An anisotropic version of the LANS- $\alpha$  equations was recently developed by Marsden and Shkoller (2001). The decaying homogeneous isotropic turbulence was considered in our previous works.<sup>4,5</sup> In this study we will focus on modeling the forced homogeneous isotropic turbulence using (LANS- $\alpha$ ) equations.

This paper is organized as follows. In the next section, a short review of the Lagrangian averaging technique is presented. The numerical technique and issues relating to forcing schemes are briefly described in Section 3. Results of our numerical experiments are presented in Section 4. A summary of our conclusions is given in Section 5.

## 2 THE LAGRANGIAN-AVERAGED NAVIER-STOKES EQUATIONS

A detailed derivation of the isotropic and anisotropic LAE- $\alpha$ /LANS- $\alpha$  equations can be found in the article by Marsden and Shkoller (2001). However, a brief summary of the relevant background material on the Lagrangian averaging approach and the resulting LAE- $\alpha$  and LANS- $\alpha$  equations is given in Mohseni *et al.*(2001).

The isotropic LANS- $\alpha$  equations in a periodic box are

$$\begin{aligned} \partial_t \mathbf{u} + (\mathbf{u} \cdot \nabla) \mathbf{u} &= -\text{grad } p + \nu \Delta \mathbf{u} + \text{Div } \tau^\alpha(\mathbf{u}), \\ \text{div } \mathbf{u} &= 0, \end{aligned} \quad (1)$$

where  $\mathbf{u}$  is the macroscopic velocity and  $\nu$  is the kinematic viscosity.  $\mathcal{S}^\alpha(\mathbf{u})$  is the *subgrid stress tensor* defined by

$$\begin{aligned} \tau^\alpha(\mathbf{u}) &= -\alpha^2(1-\alpha^2\Delta)^{-1} [ \nabla \mathbf{u} \cdot \nabla \mathbf{u}^T - \nabla \mathbf{u}^T \cdot \nabla \mathbf{u} \\ &\quad + \nabla \mathbf{u} \cdot \nabla \mathbf{u} + \nabla \mathbf{u}^T \cdot \nabla \mathbf{u}^T ]. \end{aligned} \quad (2)$$

In this equation,  $\alpha$  is a length scale of the rapid fluctuations in the flow map, below which wave activity is filtered by the nonlinear dispersion. Notice that the divergence of the last term on the right hand side can be expressed as a gradient of a scalar

$$\text{Div} (\nabla \mathbf{u}^T \cdot \nabla \mathbf{u}^T) = \text{grad} (\nabla \mathbf{u}^T : \nabla \mathbf{u}^T). \quad (3)$$

Therefore this term can be absorbed into the modified pressure  $-p$ . As with the usual Euler equations, the function  $p$  is determined from the incompressibility condition, the pressure satisfies a Poisson equation that is obtained by taking the divergence of the momentum equation.

Our Lagrangian averaging methodology permits us to use a Lagrangian generalization of G.I. Taylor's *frozen fluid hypothesis* Taylor (1938) as a turbulence closure up to  $O(\alpha^3)$  in our averaging parameter  $\alpha$ . This is made possible by averaging and asymptotically expanding at the level of the variational principle, instead of at the level of the momentum conservation equations as in the LES and RANS approaches, and considering the Lagrangian fluctuations to be frozen into the mean flow on those time scales which are required to compute temporal rates of change (time derivatives). The Taylor hypothesis is commonly invoked to compute spatial gradients in fluid turbulence experiments, and provides a natural turbulent closure in our Lagrangian averaging framework.

In this study we focus on the numerical solution of homogeneous turbulence. Our computational domain is a periodic cubic box of side  $2\pi$ . Given the number of grid points and the size of the computational domain, the smallest resolved length scale or equivalently the largest wave number,  $k_{max}$ , is prescribed. In a three-dimensional turbulent flow the kinetic energy cascades in time to smaller, more dissipative scales. The scale at which viscous dissipation becomes dominant, and which represents the smallest scales of turbulence, is characterized by the Kolmogorov length scale  $\eta$ . In a fully resolved DNS, the condition  $k_{max}\eta \gtrsim 1$  is necessary for the small scales to be adequately represented. Consequently,  $k_{max}$  limits the highest achievable Reynolds number in a direct numerical simulation for a given computational box.

The full range of scales in a turbulent flow for even a modest Reynolds number spans many orders of magnitude, and it is not generally feasible to capture them all in a numerical simulation. On the other hand, in turbulence modeling, empirical or theoretical models are used to account for the net effect of small scales on large energy-containing scales.

Direct Numerical Simulations (DNS) of isotropic flows using pseudospectral methods was pioneered by the work of Orszag and Patterson<sup>6</sup> and Rogallo.<sup>7</sup> The accuracy in the calculation of the spatial derivatives that appear in the Navier-Stokes equations is improved substantially by using pseudospectral technique as compared with the finite difference method. The core of the numerical method used in this study is based on a standard parallel pseudospectral scheme with periodic boundary conditions similar to the one described in Rogallo (1981). The spatial derivatives are calculated in the Fourier domain, while the nonlinear convective terms are computed in the physical space. The flow fields are advanced in time in physical space using a fourth order Runge-Kutta scheme. The time step was chosen appropriately to ensure numerical stability. To eliminate the aliasing errors in this procedure the two thirds rule is used, so that the upper one third of wave modes is discarded at each stage of the fourth order Runge-Kutta scheme. The resolutions of all of our DNS computations are  $170^3$  ( $256^3$  before dealiasing). In the next section, the numerical simulations of forced isotropic homogeneous turbulence based on the full DNS and LANS- $\alpha$  modeling are presented.

### 3.1 Forcing schemes

The numerical forcing of a turbulent flow is usually referred to the artificial addition of energy to the large scale (low wavenumber) velocity components in the numerical simulation. Forcing of the large scales of the flow is often used to generate a statistically stationary velocity field, in which the energy cascades to the small scales and is dissipated by viscous effects. In the statistically stationary state, the average rate of energy addition to the velocity field is equal to the average energy-dissipation rate.

In using the low wavenumber forcing, we assume that the time averaged small scale quantities are not influenced by the details of the energy production mechanisms at large scales. This assumption is closer to the truth at high Reynolds numbers, where the energy containing scales are widely separated from the dissipation scales.

The forcing parameters influence both the small scale quantities and the flow quantity variables such as the Reynolds number and the Kolmogorov length scale; however, a physically plausible forcing scheme should not influence the small scales independently of the flow quantity variables.

In order to achieve isotropic turbulence in statistical equilibrium, we use two well-studied forcing methods.

#### 3.1.1 Forcing Scheme A

The first method consists of applying forcing over a spherical shell with shell walls of unit width centered at wave number one, such that the total energy injection rate is constant in time. This forcing procedure was used by Misra and Pullin.<sup>8</sup> The forcing amplitude is adjustable via the parameter  $\delta$  while the phase of forcing is identical to that of the velocity components at the corresponding wave vectors. The Fourier coefficient of the forcing term is written as

$$\hat{f}_i = \frac{\delta}{N} \frac{\hat{u}_i}{\sqrt{\hat{u}_k \hat{u}_k^*}} \quad (4)$$

for all the modes in the specified shell. Here,  $\hat{f}_i$  and  $\hat{u}_i$  are Fourier transforms of the forcing vector  $f_i$  and velocity,  $u_i$ , in the momentum conservation equation,  $N$  is the number of wave modes that are forced. The above form of forcing ensures that the energy injection rate,  $\sum \hat{f}_i \cdot \hat{u}_i$ , is a constant which is equal to  $\delta$ . We chose  $\delta = 0.1$  for all of our runs.

### 3.1.2 Forcing Scheme B

The second method corresponds to the forcing used by Chen and Shan<sup>9</sup> where wave modes in a spherical shell  $|\mathbf{k}| = k_0$  of a certain width are forced in such a way that the forcing spectrum follows Kolmogorov's  $-5/3$  scaling law

$$\hat{f}_i = \frac{\delta}{N} \frac{\hat{u}_i}{\sqrt{\hat{u}_k \hat{u}_k^*}} k^{-5/3} \quad (5)$$

This type of forcing ensures that the energy spectrum assumes inertial range scaling starting from the lowest wave modes and thus an extended inertial range is artificially created. Imposing inertial range scaling is particularly useful for studying inertial range transfer as well as scaling laws at higher wave numbers. We have chosen  $k_0 = 2$  and  $\delta = 0.03$  in all the runs.

## 4 THE NUMERICAL EXPERIMENTS

There are three main length scales characterizing an isotropic turbulent flow: the *integral scale* characterizing the energy containing scales is defined as

$$l = \frac{3\pi}{4} \frac{\int_0^{k_{\max}} \frac{E(k)}{k} dk}{\int_0^{k_{\max}} E(k) dk}. \quad (6)$$

where  $E(k)$  is the energy spectrum function at the scalar wavenumber  $k \equiv (\vec{k} \cdot \vec{k})^{1/2}$ ; the *Kolmogorov microscale* representative of dissipative scales is

$$\eta = \left( \frac{\nu^3}{\epsilon} \right)^{1/4} \quad (7)$$

where  $\epsilon$  is the volume averaged energy-dissipation rate; the *Taylor microscale* characterizing the mixed energy-dissipation scales is defined as

$$\lambda = \sqrt{\frac{u^2}{\langle \left( \frac{\partial u_1}{\partial x_1} \right)^2 \rangle}} \quad (8)$$

where  $u$  is the root mean square value of each component of velocity defined as

$$u^2 = \frac{2}{3} \int_0^{k_{\max}} E(k) dk. \quad (9)$$

The large eddy turnover time  $T \equiv l/u$  is the time scale of the energy containing eddies.<sup>10</sup> The Taylor Reynolds number (defined based on the Taylor microscale)

$$\text{Re}_\lambda \equiv \frac{u\lambda}{\nu} \quad (10)$$

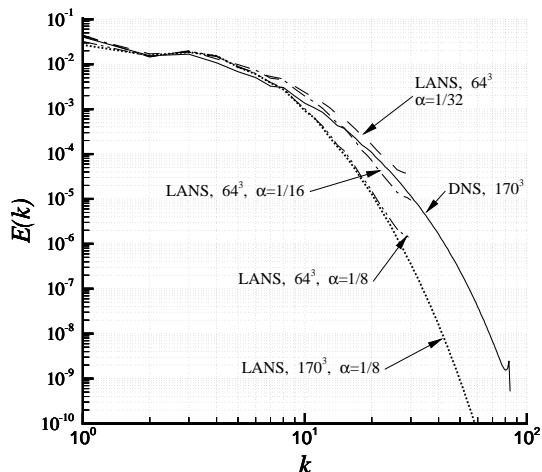


Figure 1: The energy spectra at the nondimensional time  $t = 25/0.82 = 30.5$  for forcing scheme A.

We expect that simulations which share the same value of both  $\text{Re}_\lambda$  and the nondimensional Kolmogorov length scale  $k_0\eta$  should be identical in a statistical sense.

### 4.1 Results for Forcing Scheme A

To present the results in a non-dimensional form, we use the integral length scale,  $l$ , and the root mean square of velocity,  $u$ . Throughout the forced simulations, these two quantities vary significantly; however, as equilibrium is approached, the integral length scale for the simulation with forcing scheme A approaches the value of approximately  $l \approx 0.2$ , and the root mean square of velocity is  $u \approx 0.25$ . It follows, that the corresponding eddy turnover time is  $T = l/u = 0.8$ . The computations are continued for more than 30 eddy turnover times. The equilibrium Taylor Reynolds number in these simulations is approximately 80.

The energy spectra at the nondimensional time  $t = 30.5$  is depicted in Figure 1. The total kinetic energy  $(L_2(u))$  for the DNS and LANS- $\alpha$  computations are shown in Figure 2. In these runs the flow is initialized from a fully developed turbulent flow at a higher Reynolds number. Consequently, the total kinetic energy drops as time evolves. The plot of flatness and skewness of the DNS run (shown in Figure 3) and the plot of the total kinetic energy indicate that after 10 eddy turn over times the flow is essentially in statistical equilibrium.

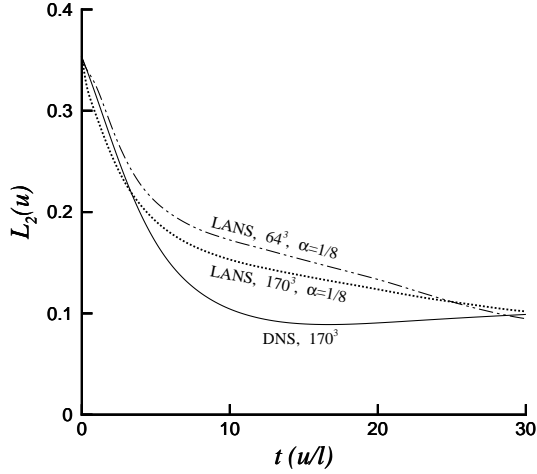


Figure 2: Total kinetic energy for forcing scheme A.

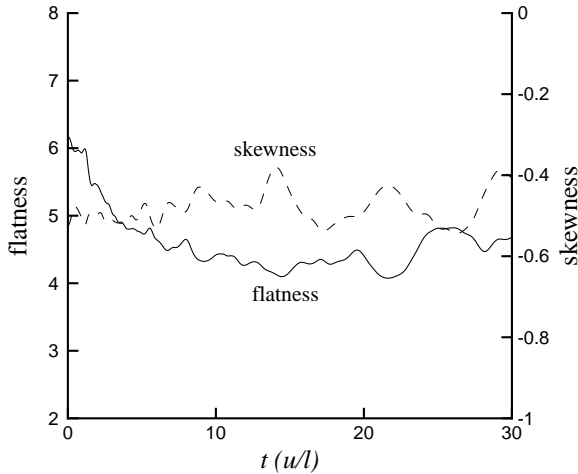


Figure 3: Flatness and skewness for forcing scheme A in the DNS run.

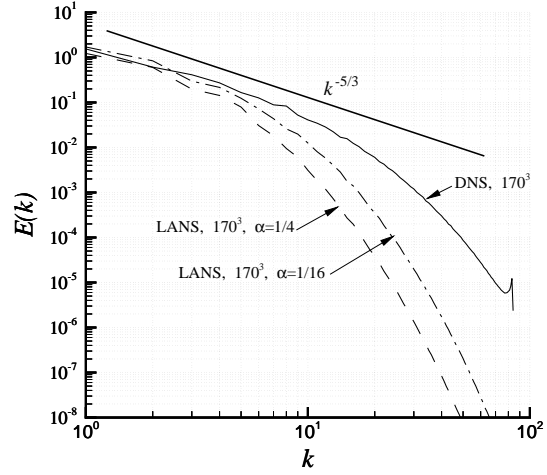


Figure 4: The energy spectra at the nondimensional time  $t = 3.25/0.23 = 14.1$  for forcing scheme B.

#### 4.2 Results for Forcing Scheme B

The integral length scale for this run is approximately  $l \approx 0.32$ , and the root mean square of velocity is  $u \approx 1.4$ . Consequently the eddy turnover time can be calculated as  $T = l/u = 0.23$ . All of the computations for the forcing scheme B are continued for almost 25 eddy turn over time. The Taylor Reynolds number,  $R_\lambda$ , is approximately 115 for these computations. The energy spectra at the nondimensional time 14.1 are shown in Figure 4. There is a well developed  $k^{-5/3}$  region over one decade in the wavenumbers. The LANS- $\alpha$  calculations at the same full resolution follows the same behavior up to the spatial scale of order  $\alpha$ , where the inverse Helmholtz operator in the LANS- $\alpha$  computations sharply steepens the energy cascades to smaller scales. While it takes a relatively long time for the total kinetic energy to settle (see Figure 5), the values of the skewness and the flatness reach an almost statistical equilibrium at around time  $t \approx 5$ , as shown in figure 6.

#### 4.3 Subgrid Transfer and Alignment of Vorticity and Subgrid Stress Eigenvectors

In order to evaluate the performance of any SGS model, it is (in principle) possible to compare the modeled SGS stress  $\tau^\alpha$  with the corresponding stress obtained by filtering DNS and computing correlation coefficients between SGS stress components. However, Piomelli *et al.*<sup>11</sup> demonstrated that such an  $a$

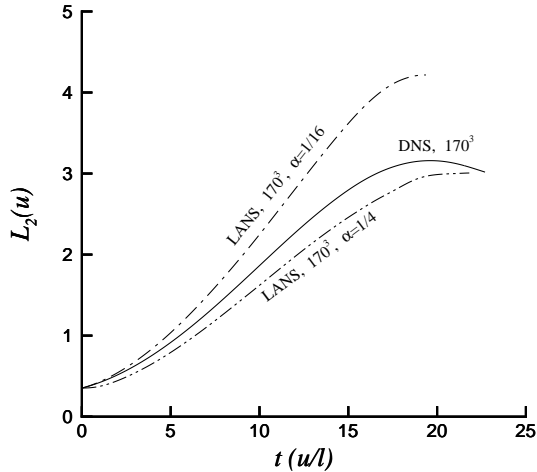


Figure 5: Total kinetic energy for forcing scheme B.

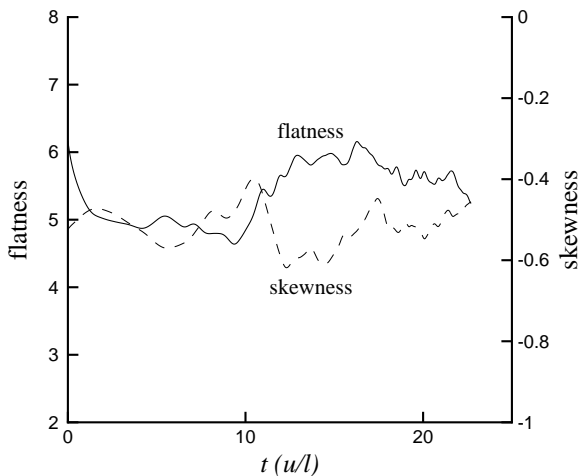


Figure 6: Flatness and skewness for forcing scheme B in the DNS run.

*priori* technique does not account for the dynamic effects of the subgrid models and therefore cannot represent a definitive test of a subgrid model.

With the development of novel experimental techniques and the availability of high resolution DNS data, it is now possible to study basic structural properties of subgrid stresses with respect to the large scale characteristics of the flow field. A three-dimensional measurement technique such as holographic particle velocimetry (HPIV) was used by Tao *et al.*<sup>12–14</sup> to study the alignment of the eigenvectors of actual and modeled components of the subgrid stresses as well as the alignments between eigenvectors of the rate of strain tensor and vorticity vector. They confirmed the preferred local alignment of the eigenvector of the rate of strain tensor corresponding to the intermediate eigenvalue with the vorticity vector, which was previously observed using pointwise DNS data.<sup>15,16</sup> They also found a preferred relative angle between the most compressive eigendirection of the rate of strain tensor and the most extensive eigendirection of the SGS tensor.

Following the work of Tao *et al.*, we will discuss the statistics of alignment between the eigenvectors of the SGS tensor  $\tau^\alpha$ , and both the eigenvectors of the rate of strain tensor,  $\mathbf{D}$ , and the unit vorticity vector,  $\boldsymbol{\omega}$ , respectively defined as

$$\mathbf{D} = \frac{1}{2} (\nabla u + \nabla u^T); \quad (11)$$

and

$$\boldsymbol{\omega} = \frac{\nabla \times u}{|\nabla \times u|}. \quad (12)$$

The actual SGS tensor,  $\tau$ , can be computed by filtering the DNS data and using the definition

$$\tau = (\overline{u \otimes u} - \bar{u} \otimes \bar{u}). \quad (13)$$

Here, overline denotes filtered quantities. We filter the DNS data by applying a wave cut-off filter with cut-off wavenumber  $k_c = 21$ , corresponding to the largest wavenumber resolved in LANS- $\alpha$  simulation with  $48^3$  grid points.

We denote the eigenvectors of  $\mathbf{D}$  by  $[\mathbf{e}_1, \mathbf{e}_2, \mathbf{e}_3]$ , ordered according to the corresponding eigenvalues  $(\lambda_1, \lambda_2, \lambda_3)$ , with  $\lambda_3 < \lambda_2 < \lambda_1$ . The eigenvectors of  $\tau^\alpha$  are  $[\mathbf{t}_1, \mathbf{t}_2, \mathbf{t}_3]$  with eigenvalues  $(\gamma_1, \gamma_2, \gamma_3)$ , such that  $\gamma_3 < \gamma_2 < \gamma_1$ . Thus, for example, we refer to  $\tilde{\mathbf{e}}_1$  as the most extensional eigendirection of  $\mathbf{D}$ , and to  $\mathbf{t}_3$  as the most compressive eigendirection of  $\tau^\alpha$ . Also,  $\tilde{\mathbf{e}}_2, \mathbf{t}_2$  are intermediate eigendirections with

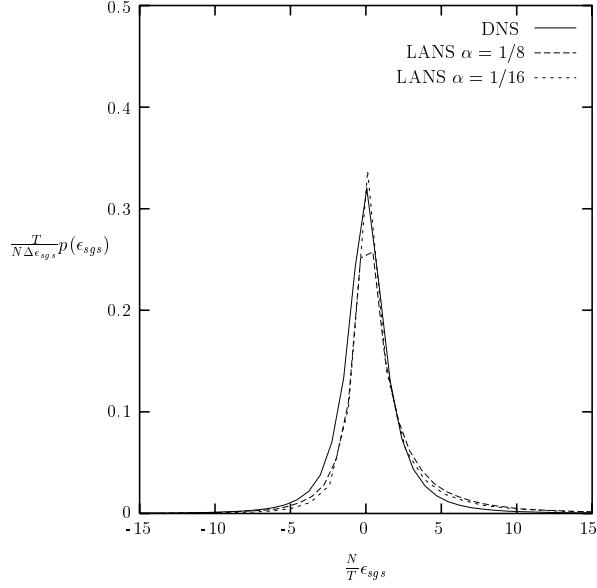


Figure 7: Probability distribution of  $\epsilon_{sgs} = \tau : \mathbf{D}$ ; solid line – Forced DNS  $170^3$  – forcing scheme A,  $Re_\lambda = 80$ ; dotted line – Forced LANS- $\alpha$   $48^3$  with  $\alpha = 1/8$  and  $\alpha = 1/16$  – forcing scheme A. The scalings are done based on the energy transfer  $T$ , sample size  $N$ , and the bin size  $\Delta\epsilon_{sgs}$ .

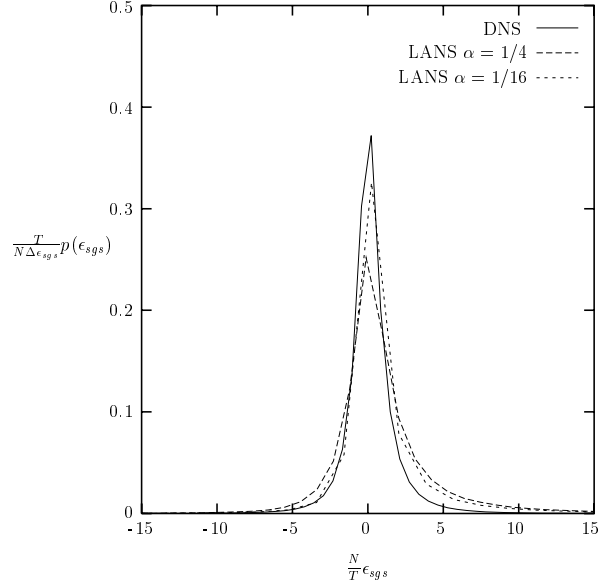


Figure 8: Probability distribution of  $\epsilon_{sgs} = \tau : \mathbf{D}$ ; solid line – Forced DNS  $170^3$  – forcing scheme B,  $Re_\lambda = 80$ ; dotted line – Forced LANS- $\alpha$   $64^3$  with  $\alpha = 1/4$  and  $\alpha = 1/16$  – forcing scheme B. The scalings are done based on the energy transfer  $T$ , sample size  $N$ , and the bin size  $\Delta\epsilon_{sgs}$ .

corresponding intermediate eigenvalues  $\lambda_2$ ,  $\gamma_2$ , respectively.

We remark that commonly used linear, Smagorinsky-type, SGS models implicitly assume that the eigenvectors of the SGS stress are locally aligned with the eigenvectors of the rate of strain tensor, which is contrary to the experimental evidence.

We first used  $170^3$  DNS data obtained using forcing scheme A and the data from  $48^3$  LANS- $\alpha$  simulation to compute the distribution of the energy transfer,  $e_{sgs} = \tau : \mathbf{D}$ , due to the contribution of the subgrid term. The distributions are presented in Figure 7. In Figure 8, the same energy transfer is computed for the cases with the forcing scheme B. Using the same data sets we computed the distributions of the alignment (cosine of the angles) between the eigenvectors of the rate of strain tensor and vorticity vector as well as the SGS tensor.

We first used forcing scheme A and LANS- $\alpha$  simulations with  $64^3$  grid points and  $\alpha = 1/8$ . Figures 9 and 11 indicate that in the LANS- $\alpha$  simulations, the preferential alignment between the vorticity vector and the eigendirection of the rate of strain tensor

corresponding to the intermediate eigenvalue is not as pronounced as in DNS. As can be seen in Figures 10 and 12 the eigenvectors of the modeled subgrid tensor  $\tau^\alpha$  display qualitatively similar alignment as that computed from DNS data. In particular, experimentally observed preferred angle between  $\mathbf{e}_3$  and  $\mathbf{t}_1$  is captured by the LANS- $\alpha$  model. Similar observations can be made base on the simulations where the forcing scheme B was used. For these cases, probability distributions of the cosine of the angles between eigenvectors and the vorticity vector are obtained by filtering the DNS data using a wave cut-off filter with cut-off wavenumber  $k_c = 32$  and is given in Figures 13 and 14. These results are compared to LANS- $\alpha$  results corresponding to simulations with  $64^3$  grid points and  $\alpha = 1/16$  which are presented in Figures 15 and 16.

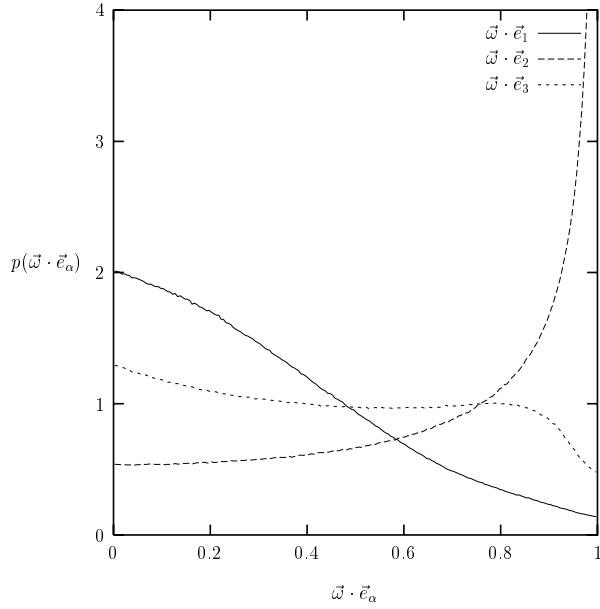


Figure 9: Probability distribution of  $\vec{\omega} \cdot \vec{e}_\alpha$ ; Forced DNS  $170^3$  – forcing scheme A;  $Re_\lambda = 80$ .

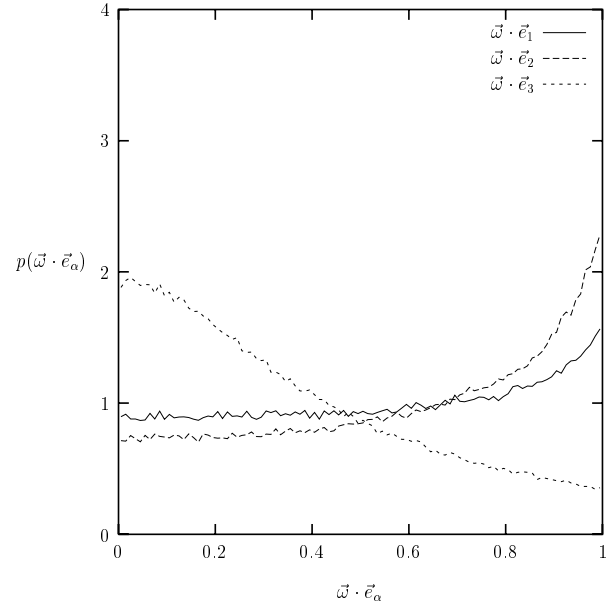


Figure 11: Probability distribution of  $\vec{\omega} \cdot \vec{e}_\alpha$ ; Forced LANS- $\alpha$   $48^3$  with  $\alpha = 1/8$  – forcing scheme A.

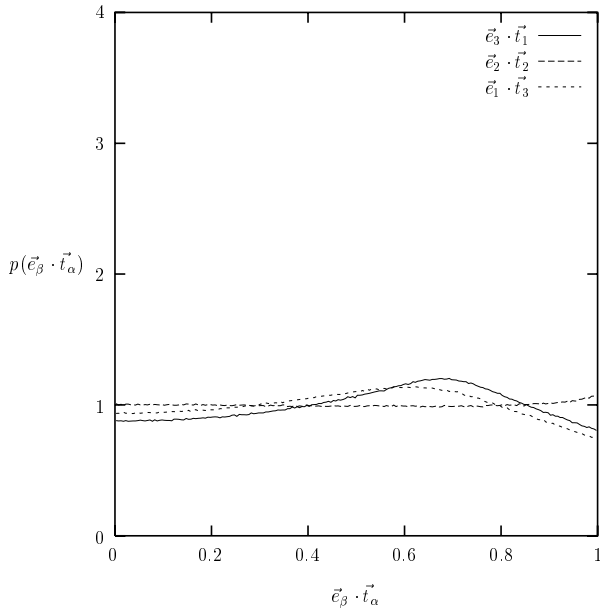


Figure 10: Probability distribution of  $\vec{e}_1 \cdot \vec{t}_3$ ,  $\vec{e}_2 \cdot \vec{t}_2$ , and  $\vec{e}_3 \cdot \vec{t}_1$ ; Forced DNS  $170^3$  – forcing scheme A;  $Re_\lambda = 80$ .

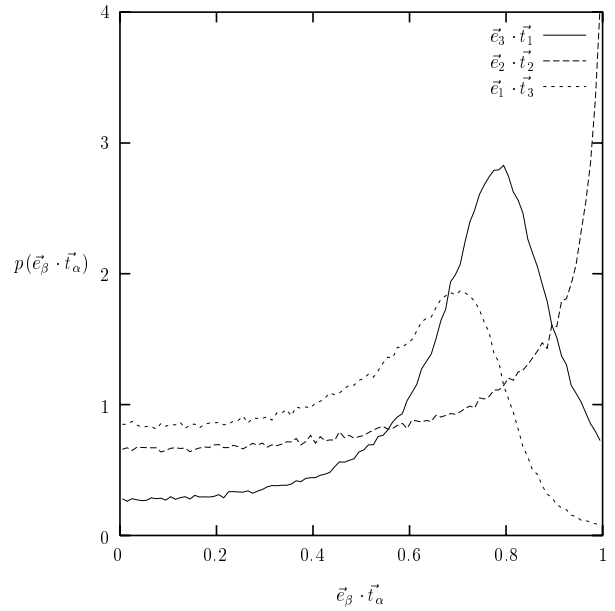


Figure 12: Probability distribution of  $\vec{e}_1 \cdot \vec{t}_3$ ,  $\vec{e}_2 \cdot \vec{t}_2$ , and  $\vec{e}_3 \cdot \vec{t}_1$ ; Forced LANS- $\alpha$   $48^3$  with  $\alpha = 1/8$  – forcing scheme A.

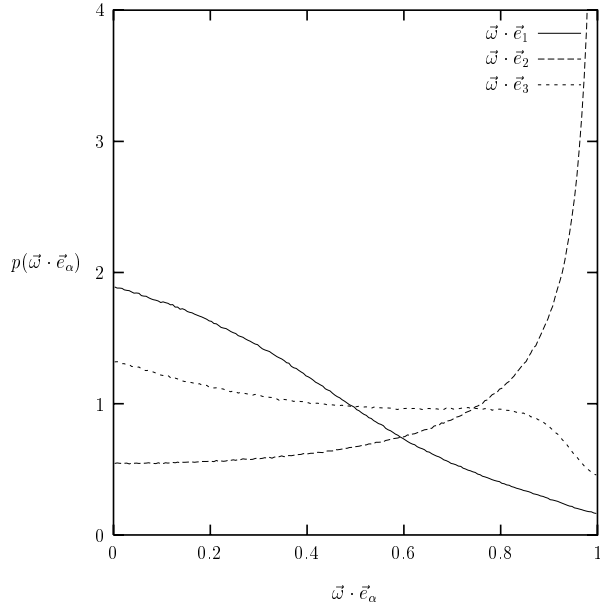


Figure 13: Probability distribution of  $\vec{\omega} \cdot \vec{e}_\alpha$ ; Forced DNS  $170^3$  – forcing scheme B;  $Re_\lambda = 80$ .

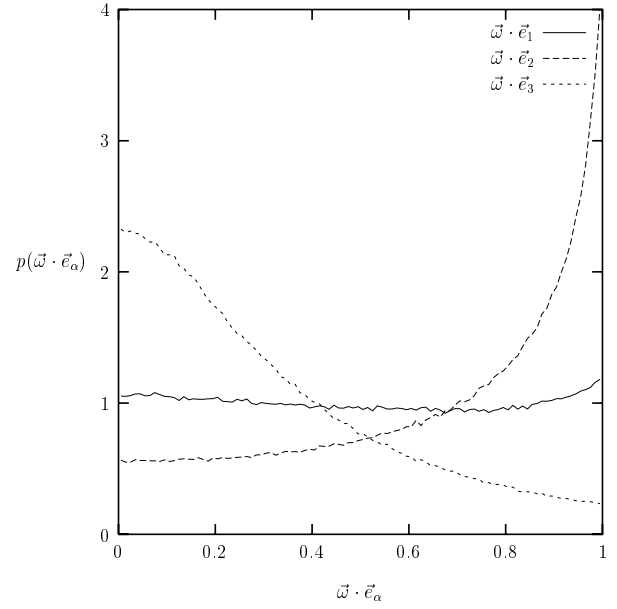


Figure 15: Probability distribution of  $\vec{\omega} \cdot \vec{e}_\alpha$ ; Forced LANS- $\alpha$   $64^3$  with  $\alpha = 1/16$  – forcing scheme B.

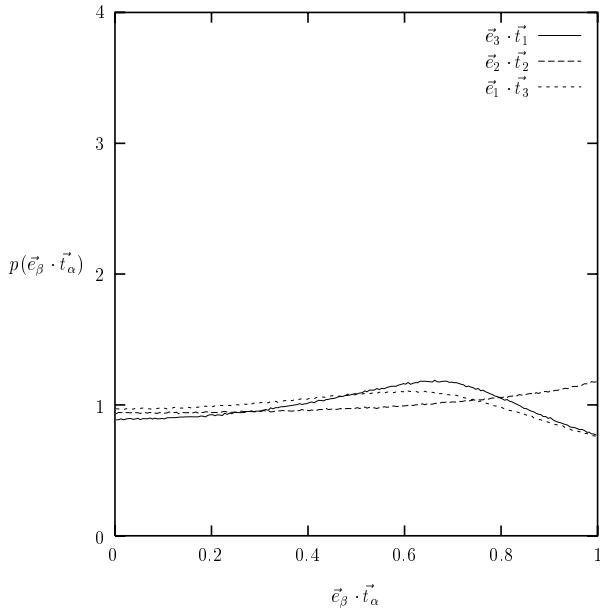


Figure 14: Probability distribution of  $\vec{e}_1 \cdot \vec{t}_3$ ,  $\vec{e}_2 \cdot \vec{t}_2$ , and  $\vec{e}_3 \cdot \vec{t}_1$ ; Forced DNS  $170^3$  – forcing scheme B;  $Re_\lambda = 80$ .

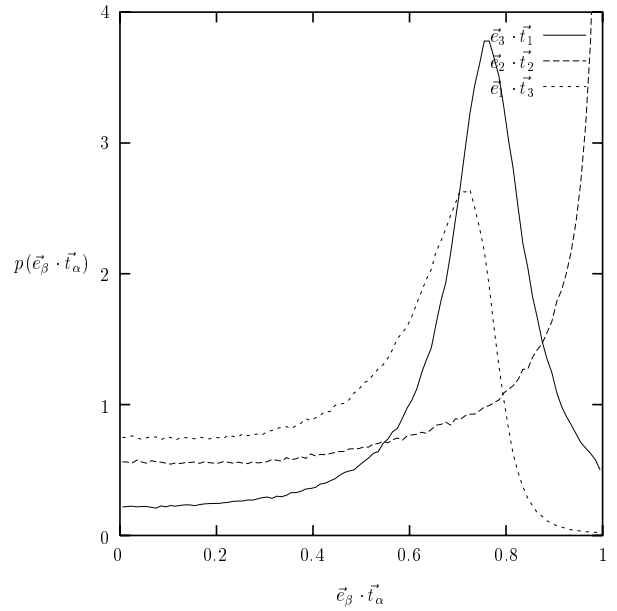


Figure 16: Probability distribution of  $\vec{e}_1 \cdot \vec{t}_3$ ,  $\vec{e}_2 \cdot \vec{t}_2$ , and  $\vec{e}_3 \cdot \vec{t}_1$ ; Forced LANS- $\alpha$   $64^3$  with  $\alpha = 1/16$  – forcing scheme B.

We performed a set of forced isotropic turbulence simulations of the LANS- $\alpha$  equations and studied their equilibrium states. The results of the LANS- $\alpha$  simulations were compared to the results obtained from high-resolution DNS simulations, characterized by the equilibrium Taylor Reynolds numbers  $Re_\lambda = 80$  and 115 for two different forcing schemes. We studied the effect of varying the model length-scale  $\alpha$ . The key feature of the Lagrangian averaging technique is the dispersive (not dissipative) fashion in which it decays energy in inviscid Lagrangian-Averaged Euler (LAE- $\alpha$ ) equations. In the LANS- $\alpha$  equations, the dispersive decay is accompanied by the same viscous dissipation as appears in the original Navier-Stokes equations. Therefore, as can be seen from equation (1), the LANS- $\alpha$  equations on a periodic box are given by a subgrid stress addition to the usual Navier-Stokes equations, and this subgrid stress  $\tau^\alpha$  affects the energy transfer via nonlinear dispersion.  $\tau^\alpha$  depends on the length scale  $\alpha$ , and limits the effect of vortex stretching, causing the energy spectrum to fall-off rapidly for scales smaller than  $\alpha$ . The slope of this drop at higher wave-modes can be predicted by an argument similar to Kolmogorov's  $k^{-5/3}$  in the inertial range.

The equilibrium energy spectrum in our LANS- $\alpha$  simulations were in good agreement with the DNS data. Our simulations, in agreement with previous results by Chen *et al.*,<sup>17</sup> show dependence of the equilibrium turbulence spectra on the model length scale  $\alpha$ . At the wavenumber  $k \approx 1/\alpha$  the slope of the spectra changes from the inertial range slope to a much steeper slope. Even with  $170^3$  grid-point LANS- $\alpha$  simulations due to the insufficient resolution we were not able to determine the actual slope and confirm or falsify its existing estimates. Our study of the alignment of the vorticity vector and the eigenvectors of the rate of strain tensor with the eigenvectors of the subgrid stress tensor showed a basic qualitative agreement of the LANS- $\alpha$  results with the filtered DNS data. We observed that the probability densities of the energy transfer due to the LANS- $\alpha$  subgrid model is in a good quantitative agreement with the corresponding probability density obtained from the DNS.

## REFERENCES

- [1] R.S. Rogallo and P. Moin. Numerical simulations of turbulent flows. *Ann. Rev. Fluid Mech.*, 16:99–137, 1984.

- [2] C. Canuto, M.Y. Hussaini and A. Quarteroni, and T.A. Zang. *Spectral Methods in Fluid Dynamics*. Springer Series in Computational Physics. Springer-Verlag, Berlin, 1988.
- [3] A.N. Kolmogorov. The local structure of turbulence in incompressible viscous fluids at very large Reynolds numbers. *Dokl. Nauk. SSSR.*, 30:301–305, 1941.
- [4] K. Mohseni, B. Kosovic, J. Marsden, S. Shkoller, D. Carati, A. Wray, and B. Rogallo. Numerical simulations of homogeneous turbulence using Lagrangian averaged Navier-Stokes equations. In *Proceedings of the 2000 Summer Program*, pages 271–283. NASA Ames/Stanford Univ., 2000.
- [5] K. Mohseni, S. Shkoller, B. Kosovic, and J. Marsden. Numerical simulations of the Lagrangian Averaged Navier-Stokes (LANS) equations. In *Second International Symposium on Turbulence and Shear Flow Phenomena*, Stockholm, Sweden, July 2001. KTH.
- [6] S.A. Orszag and G.S. Patterson. *Statistical Models and Turbulence*, volume 12 of *Lecture Notes in Physics*, chapter Numerical simulation of turbulence. Springer, New York, 1972.
- [7] R.S. Rogallo. Numerical experiments in homogeneous turbulence. In *NASA Tech. Memo 81315*, 1981.
- [8] A. Misra and D.I. Pullin. A vortex-based subgrid stress model for large-eddy simulation. *Phys. Fluids*, 9(8):2443–2454, 1997.
- [9] S. Chen and X. Shan. High-resolution turbulent simulations using the connection machine-2. *Comp. Phys.*, 6(6):2443–2454, 1992.
- [10] G.K. Batchelor. *The Theory of Homogeneous Turbulence*. Cambridge University Press, Cambridge, 1953.
- [11] U. Piomelli, P. Moin, and J. Ferziger. Model consistency in large eddy simulation of turbulent channel flows. *Phys. Fluids*, 31:1884–1891, 1988.
- [12] B. Tao, J. Katz, and C. Meneveau. Application of HPIV data of turbulent duct flow for turbulence modelling. In *Proceedings of 3rd ASME/JSME Joint Fluids Engineering Conference*. ASME, June 18-22 1999.

- [13] B. Tao, J. Katz, and C. Meneveau. Effects of strain-rate and subgrid dissipation rate on alignment trends between large and small scales in turbulent duct flow. In *Proceedings of 3rd ASME FEDSM'00, Fluids Engineering Division Summer Meeting*. ASME, June 11-15 2000.
- [14] B. Tao, J. Katz, and C. Meneveau. Geometry and scale relationships in high reynolds number turbulence determined from three-dimensional holographic velocimetry. *Phys. Fluids*, 12:941–944, 2000.
- [15] R.M. Kerr. Higher-order derivative correlations and the alignment of small-scale structures in isotropic numerical turbulence. *J. Fluid Mech.*, 153:31–58, 1985.
- [16] W.T. Ashurst, A.R. Kerstein, R.M. Kerr, and C.H. Gibson. Alignment of vorticity and scalar-gradient in simulated Navier-Stokes turbulence. *Phys. Fluids*, 30:2343–2353, 1987.
- [17] S.Y. Chen, D.D. Holm, L.G. Margoin, and R. Zhang. Direct numerical simulations of the navier-stokes alpha model. *Physica D*, 133:66–83, 1999.